

## Research Article

# Humanoid Robot Teleoperation Through 3-D Pose Estimation

Jacobo E. Cruz-Silva<sup>1</sup>, R. Sivaraman<sup>2\*</sup>, J. Yaljá Montiel-Pérez<sup>1</sup>, J. Humberto Sossa-Azuela<sup>1</sup>, J. López-Bonilla<sup>3</sup>

<sup>1</sup>National Polytechnic Institute, Computer Research Center, AV. Juan de Dios Batiz S/N, Nueva Industrial Vallejo, 07738 Gustavo A. Madero, Mexico City, Mexico

<sup>2</sup>Department of Mathematics, Dwaraka Doss Goverdhan Doss Vaishnav College, Chennai, India

<sup>3</sup>Sime Zacatenco, National Polytechnic Institute, EDIF. 4, 1. Piso, Col. Lindavista 07738, CDMX, Mexico  
Email: rsivaraman1729@yahoo.co.in

**Received:** 12 August 2023; **Revised:** 24 November 2023; **Accepted:** 18 January 2024

**Abstract:** The knowledge of how the human motions is performed helps to understand how the human body works. This paper presents a method to estimate the human limbs angles through a kinematic model depicted by Roll-Pitch-Yaw rotationmatrix and the mimic of those angles on a humanoid robot. The advantage of this model is the detailed representation of each joint movement in the coordinate axes  $(x, y, z)$ . The angles estimation is made with the information provided by algorithms of artificial vision and artificial intelligence. In order to reduce the latency between the human motion capture and robot motions, a fuzzy logic controller is implemented in order to control each robot joint. The final robot limbs angles are compared with the human angles in order to obtain the final error between those measurements. This method shows a similar result on the arms posture regarding previous works.

**Keywords:** fuzzy control, human body, kinematics, modeling, NAO robot, Roll-Pitch-Yaw, speed profile

**MSC:** 68T40, 93C85, 70B15

## 1. Introduction

The study of human upper and lower limbs motions is relevant for several areas. For the robot teleoperation area, it is important to know how the human body moves in order to mimic those movements through Haptic devices [1-9] or artificial vision [10-12] that captures the human motion. In Health Sciences, the human motion replication is applied to create new rehabilitation therapies [13-15].

In the present paper, a method to mimic the human limbs angles on a humanoid robot using three-dimensional kinematic model and a fuzzy logic control algorithm is described.

There are several methods to create kinematic mode, such as: Denavit-Hartenberg convention, through quaternities Roll-Pitch-Yaw matrices, The last mentioned are the matrices used on this method. this array contains the points obtained by three-dimensional analysis of 4 plain images that are taken from 4 different points of view (front, back, right side, left side) instead of a 3-D approximation [16] from a single point of view of a 2-dimensional image.

Then, the limbs angles are estimated by three equations which are derived from the kinematic model and are the set

points of the fuzzy control algorithm of the robot. The fuzzy logic algorithms are Mamdani fuzzy inference systems with “if, then” rules engine Figure 1.

The present work is focused on a possible real application, due this, the fuzzy logic controller is a good option to be implemented on a real time controller system due the low complexity.

The artificial intelligence algorithm [16] obtains the information of four cameras equipped with two different sensors, RGB sensor and Depth sensor. The images captured by the 4 RGB sensors are processed with a Convolutional Neural Network which creates feature maps of input image and infers 2-D key points for person in the image.

After that, the 3-D points are calculated making the relation between four set of 2-D points. The artificial intelligence algorithm [16] provides a robust method to detect the joint’s location. The measurements are not affected by the lighting changes and it was not necessary to use special equipment on the body, that is the main advantage of the algorithm.

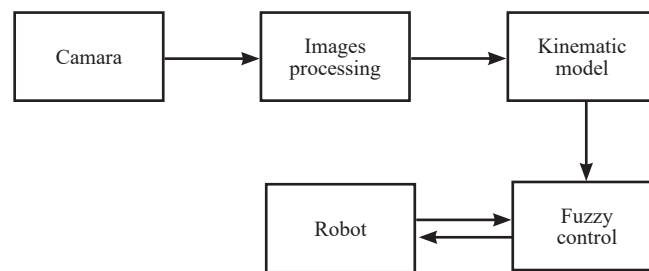


Figure 1. Diagram of NAO robot teleoperation process

The main contribution of this method is the new manner to estimate the human limbs position through artificial intelligence and teleoperated a robot with less computing complexity control algorithm (fuzzy logic controller) that is suitable to be applied on real-time systems for a real application.

## 2. Method

### 2.1 Kinematic model

The five main movements that can be made by the human and the NAO robot are the following [17]:

Flexion. It is angle decrease at one joint Figure 2.

Extension. It is angle increase at one joint Figure 3.

Abduction. It is the motion of a limb away from the midline of the body Figure 3.

Adduction. It is the motion of a limb toward to the midline of the body Figure 3.

Rotation. It is the motion around a longitudinal axis of a bone, it can be internal or external Figure 3.

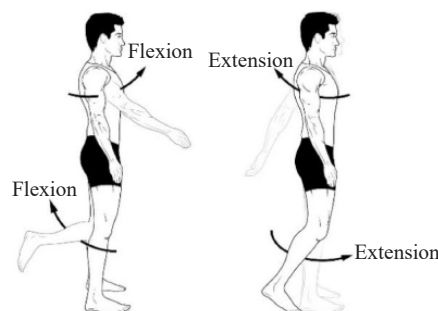
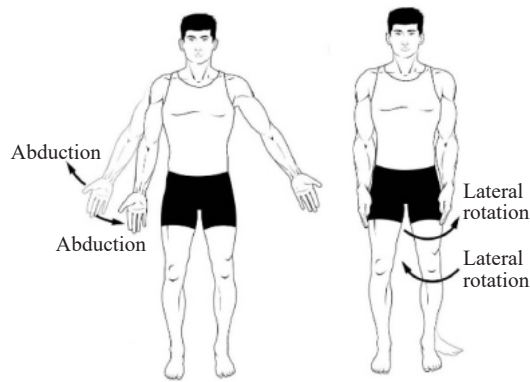
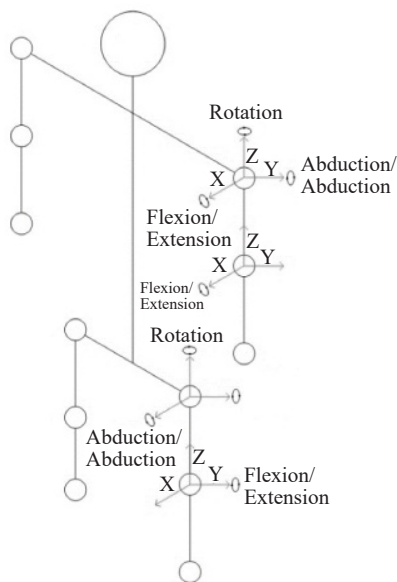


Figure 2. Flexion and extension movements



**Figure 3.** Abduction, adduction and rotation movements

The motion of upper limbs considered in this method were the shoulders and elbows motions. The shoulder motions are Flexion/Extension ( $x$ ), Abduction/Adduction ( $y$ ) and Rotation ( $z$ ). For the lower limbs, the hip motions are Flexion/Extension ( $y$ ), Abduction/Adduction ( $x$ ) and Rotation ( $z$ ), the knee motions are only the Flexion/Extension ( $y$ ) as is shown on the Figure 4.



**Figure 4.** Upper and lower limb joints

In order to describe the motions previously mentioned, the Roll, Yaw and Pitch rotation matrices were selected. The Eq. (1) is the rotation matrix on the ( $z$ ) axis (Yaw) and the Eq. (2) is the rotation matrix on the ( $y$ ) axis (Pitch) and the Eq. (3) is the rotation matrix on the ( $x$ ) axis (Roll).

$$R_z = \begin{bmatrix} C_\varphi & -S_\varphi & 0 \\ S_\varphi & C_\varphi & 0 \\ 0 & 0 & 1 \end{bmatrix} \quad (1)$$

$$R_y = \begin{bmatrix} C_\theta & 0 & S_\theta \\ 0 & 1 & 0 \\ -S_\theta & 0 & C_\theta \end{bmatrix} \quad (2)$$

$$R_x = \begin{bmatrix} 1 & 0 & 0 \\ 0 & C_\psi & -S_\psi \\ 0 & S_\psi & C_\psi \end{bmatrix} \quad (3)$$

Where  $C_\phi$ ,  $C_\theta$  and  $C_\psi$  represent  $\cos_\phi$ ,  $\cos_\theta$  and  $\cos_\psi$  respectively and  $S_\phi$ ,  $S_\theta$  and  $S_\psi$  represent  $\sin_\phi$ ,  $\sin_\theta$  and  $\sin_\psi$  respectively.

Due the shoulders and hips are able to perform rotations on the 3 axis, the 3 previous equations were multiplied to obtain a single rotation matrix, Eq. (4).

$$R_{xyz} = \begin{bmatrix} C_\phi C_\theta & -S_\phi C_\psi + C_\phi S_\theta S_\psi & S_\phi S_\psi + C_\phi S_\theta S_\psi \\ S_\phi C_\theta & C_\phi C_\psi + S_\phi S_\theta S_\psi & -C_\phi S_\psi + S_\phi S_\theta S_\psi \\ S_\theta & C_\theta S_\psi & C_\theta C_\psi \end{bmatrix} \quad (4)$$

The artificial intelligence algorithm [16] is able to locate 15 key points. Three of these key points were used as reference point (0, 1, 14) and the others key points were used to estimate the joints angles. These key points are shown on the Figure 5.

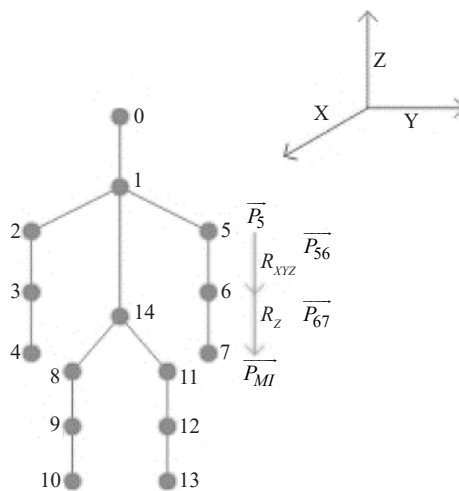


**Figure 5.** Abduction, adduction and rotation movements

The kinematic model of the lower and upper limbs, specifically the arms and legs, is described by the following equations:

$$\overline{P_{MD}} = R_x \overline{P_{34}} + R_{xyz} \overline{P_{23}} + \overline{P_2} \quad (5)$$

$$\overline{P_{MI}} = R_x \overline{P_{67}} + R_{xyz} \overline{P_{56}} + \overline{P_5} \quad (6)$$

$$\overline{P_{TD}} = R_y \overline{P_{910}} + R_{xyz} \overline{P_{89}} + \overline{P_8} \quad (7)$$

$$\overline{P_{TI}} = R_y \overline{P_{1213}} + R_{xyz} \overline{P_{1112}} + \overline{P_{11}} \quad (8)$$

Where Eq. (4) describes the final position of the right arm with the vector  $\overline{P_{MD}}$  (MD is the acronym for Right Hand in Spanish). The equation is composed of a translation from the point of origin  $P_0 = [0 \ 0 \ 0]^T$ , the point 0 shown in Figure 5, to the point 2 creating the vector  $\overline{P_2}$ . A second translation from the point 2 to the point 3 creates the vector  $\overline{P_{23}}$ . This second vector is able to rotate in the three axes  $(x, y, z)$ , these rotations are described in the rotation matrix  $R_{xyz}$ . Finally, a translation to the point 4 creates the vector  $\overline{P_{34}}$ , this final vector only can rotate in the  $(x)$  axis, which is described by the rotation matrix  $R_x$ . This same procedure is applied for the other limbs, where Eq. (5) corresponds to the left arm (MI, left hand in Spanish), Eq. (6) to the right leg (TD, right ankle in Spanish) and Eq. (7) corresponds to the left leg (TI left ankle in Spanish). The points mentioned above are the points described in Figure 5.

In the Table 1 and Table 2 are shown the maximum angles that human limbs can perform before get injured, those angles are also called as comfort angles [17].

**Table 1.** Comfort angles of the body right limbs

Part	Movement	Axis	ID	Angle range
Shoulder	Flexion/Extension	X	$q_1$	-150° to 40°
	Abduction/Adduction	Y	$q_2$	-150° to 20°
	Rotation	Z	$q_3$	-70° to 60°
Elbow	Flexion/Extension	X	$q_4$	10° to 150°
	Flexion/Extension	Y	$q_5$	-130° to 15°
Hip	Abduction/Adduction	X	$q_6$	-45° to 20°
	Rotation	Z	$q_7$	-50° to 45°
Knee	Flexion/Extension	Y	$q_8$	0° to 155°

**Table 2.** Comfort angles of the body left limbs

Part	Movement	Axis	ID	Angle range
Shoulder	Flexion/Extension	X	$q_9$	-150° to 40°
	Abduction/Adduction	Y	$q_{10}$	-20° to 150°
	Rotation	Z	$q_{11}$	-70° to 60°
Elbow	Flexion/Extension	X	$q_{12}$	-150° to 10°
	Flexion/Extension	Y	$q_{13}$	-130° to 15°
Hip	Abduction/Adduction	X	$q_{14}$	-20° to 45°
	Rotation	Z	$q_{15}$	-50° to 45°
Knee	Flexion/Extension	Y	$q_{16}$	0° to 155°

The vector value of each limb was calculated by the Eq. (9).

$$\overline{V}_{ext} = \begin{bmatrix} (X_e - X_0) \\ (Y_e - Y_0) \\ (Z_e - Z_0) \end{bmatrix} = \begin{bmatrix} X_{ext} \\ Y_{ext} \\ Z_{ext} \end{bmatrix} \quad (9)$$

Where,  $(X_0, Y_0, Z_0)$  are the limb origin points and  $(X_e, Y_e, Z_e)$  are the end points. For example, the origin of the forearm is the elbow and the end is the wrist.  $\overline{V}_{ext}$  is the final vector of the limb with the points  $(X_{ext}, Y_{ext}, Z_{ext})$ .

In order to obtain the motion angles, we selected the directional cosines to estimate the rotation angles  $q_n$  on the different axis, where  $q_n$  is the ID of angles shown in the Tables 1 and 2. The director cosine for the rotation angle at the (x) axis is the Eq. (10) and for the (y) and the (z) axis are the Eq. (11) and Eq. (12) respectively.

$$q_n = \cos^{-1} \left( \frac{Y_{ext}}{|\overline{V}_{ext}|} \right) \quad (10)$$

$$q_n = \cos^{-1} \left( \frac{Z_{ext}}{|\overline{V}_{ext}|} \right) \quad (11)$$

$$q_n = \cos^{-1} \left( \frac{Z_{ext}}{|\overline{V}_{ext}|} \right) \quad (12)$$

Where  $Y_{ext}$  corresponds to the (y) point from vector  $\overline{V}_{ext}$  and  $|\overline{V}_{ext}|$  is the module of that vector. In the same way,  $X_{ext}$  and  $Z_{ext}$  correspond to (x) and (y) points from the.

## 2.2 Control algorithm

The control algorithm selected for this method is a Fuzzy PD (Proportional Derivative) controller Figure 6. This controller is a Mamdani Fuzzy Inference System which is based on “if-then” inference engine. For this application, the hiprotations were excluded due the NAO robot is not able to perform this motion. The controller’s set-points were bounded to the angle values in the Tables 1 and 2 in order to prevent a damage at the robot joints. In order to control the 14 joints, it was applied 14 control loops like the one described in the Figure 1 running on a concurrent way.

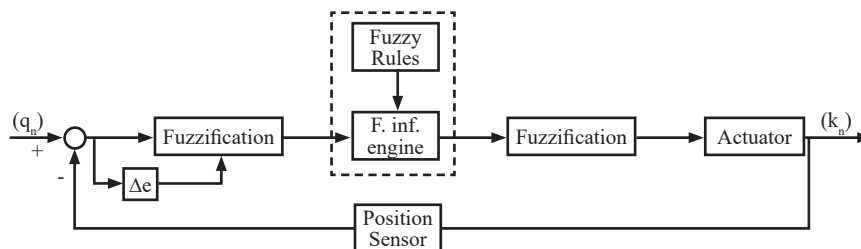


Figure 6. Fuzzy controller

In the first step, the values to error and differential error through input membership function were assigned. The error was estimated subtracting the set-point and the angle measured by the sensors in robot’s joints at an instance of time  $(e(t))$

and the differential error is  $(\Delta e(t) = e(t) - e(t - 1))$ .

The error and the differential error were inradian and could be positive and negative, duethis, five triangular memberships functions wereassigned as follow:

- **eng.** Big Negative Error.
- **enb.** Low Negative Error.
- **ec.** Zero Error.
- **epg.** Big Positive Error.
- **epb.** Low Positive Error.

The robots manufactured provided the option to control the speed of each limb with values from 0 to 1, which 0 is zero speed and 1 isthe maximum speed.Five triangular membershipsfunctions were defined in this range as follow

- **vc.** Zero Speed.
- **vb.** Low Speed.
- **vm.** Medium Speed.
- **va.** High Speed.
- **vmx.** Maximum Speed.

The inference engine was defined with the rules shown in the Table 3. The fuzzy rules were designed to smoothly decrease the speed when the joint approaches to the set point. This behavior is shown on the control surface in Figure 7. Finally, the values that was sent to the robot were estimated by the Center of Gravity (CoG) defuzzification method Eq. (12).

$$x = \frac{\sum_{i=1}^n \mu_{\bar{c}}(x_i) \cdot x_i}{\sum_{i=1}^n \mu_{\bar{c}}(x_i)} \tag{13}$$

Where  $x$  is the crisp value,  $\mu_{\bar{c}}$  is the membershipfunction and  $x_i$  output variable.

**Table 3.** Fuzzy rules

E/ΔE	eng	enb	ec	epb	epg
eng	vmx	va	vm	va	vmx
enb	va	vm	vb	vm	va
ec	vm	vb	vc	vb	vm
epb	va	vm	vb	vm	va
epg	vmx	va	vm	va	vmx

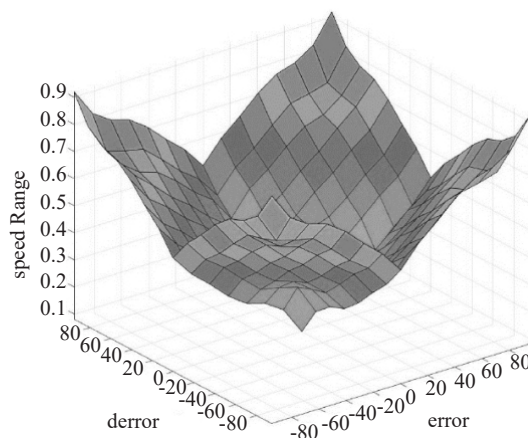


**Figure 7.** Control surface

The fuzzy rules are defined as the next example, based on the information contained in the Table 3:

$$IF E = eng \text{ AND } \Delta E = enb \text{ THEN Output} = va$$

### 3. Results

The tests were divided into: stable postures test and unstable posture test. The stable posture was defined as the posture when the body's center of mass is located at the support base, the human can perform this posture without loss the balance.

The unstable posture was when the body's center of mass is not located at the support base. For this specific posture, the tests were divided into free unstable posture and intervened unstable posture. When a person lifted the robot in order to avoid the feet touch the ground was knew as intervened unstable posture. if the robot's feet touch the ground, it is a free unstable posture.

The errors were calculated subtracting the final angles from the human limbs and the robot limbs. These angles are shown in the Tables 1 and 2.

$$E_{RMA(n)} = \frac{|k_{(n)} - q_{(n)}|}{1 - |q_{(n)}|} \quad (14)$$

$$E_{RTP} = \frac{E_{RMA(1)} + \dots + E_{RMA(14)}}{14} \quad (15)$$

The Eq. (14) is the Relative Angle Error ( $E_{RMA(n)}$ ), where  $k_{(n)}$  is the angle from robot joint and  $q_{(n)}$  is the angle from the human joint. The Eq. (15) is the Total Position Error ( $E_{RTP}$ ) and is the average of each Relative Angle Error from the 14 key point.

On the first test, the person was asked to perform a stable posture. The person extended his arms and did not move the legs, In Figure 8. The robot final posture and the 3-D reconstruction are shown in Figure 9 and Figure 10, respectively. The Table 4 contains the errors from each limb's angle.



Figure 8. Stable posture-Human pose

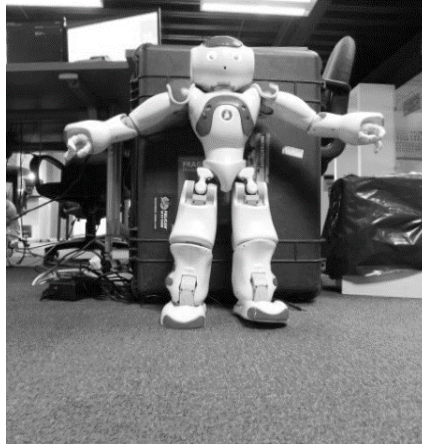


Figure 9. Stable posture-NAO pose

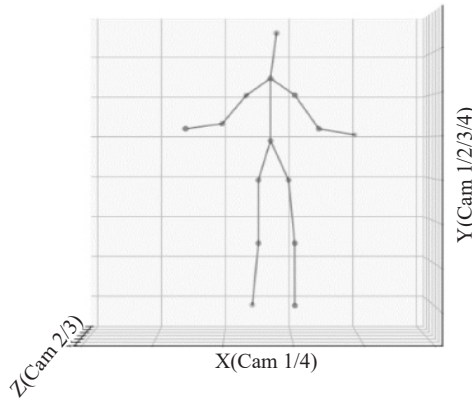


Figure 10. Stable posture-3-D skeleton

Table 4. Errors in stable posture

Part	Axis/ID right part	Error Person-NAO (%)	Axis/ID left part	Error Person-NAO (%)
Shoulder	$Xq_1-k_1$	15.3593	$Xq_9-k_9$	3.6016
	$Yq_2-k_2$	13.1042	$Yq_{10}-k_{10}$	16.9010
	$Zq_3-k_3$	4.2484	$Zq_{11}-k_{11}$	1.9413
Elbow	$Xq_4-k_4$	9.4681	$Xq_{12}-k_{12}$	13.2249
Hip	$Yq_5-k_5$	32.2980	$Yq_{13}-k_{13}$	19.3410
	$Xq_6-k_6$	33.6234	$Xq_{14}-k_{14}$	26.9505
Knee	$Yq_8-k_8$	4.5920	$Yq_{16}-k_{16}$	16.5909

On the second test, the person raised one leg and extend the arms slightly and the robot stayed on the ground because it was a free unstable posture, Figure 11. The robot's anti-fall safety system located at the feet was activated automatically lowering the legs to the ground in order to avoid a fall. The robot final posture and the 3-D reconstruction are shown in Figure 12 and Figure 13, respectively. The Table 5 contains the errors from each limb's angle.



**Figure 11.** Free unstableposture-Human pose



**Figure 12.** Free unstableposture-NAO pose

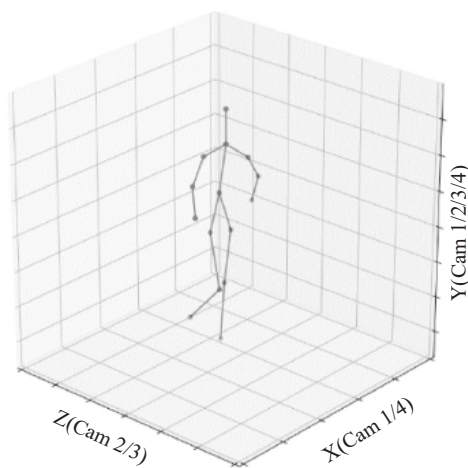


**Figure 13.** Free unstableposture-3-D skeleton

**Table 5.** Errors in free unstable posture

Part	Axis/ID right part	Error Person-NAO(%)	Axis/ID left part	Error Person-NAO(%)
Shoulder	$Xq_1-k_1$	22.5545	$Xq_9-k_9$	31.8723
	$Xq_2-k_2$	15.2686	$Xq_{10}-k_{10}$	53.1763
	$Xq_3-k_3$	25.7007	$Xq_{11}-k_{11}$	21.2021
Elbow	$Xq_4-k_4$	17.3055	$Xq_{12}-k_{12}$	63.7488
Hip	$Xq_5-k_5$	27.9923	$Xq_{13}-k_{13}$	56.8126
	$Xq_6-k_6$	44.0163	$Xq_{14}-k_{14}$	96.9256
Knee	$Xq_8-k_8$	30.0295	$Xq_{16}-k_{16}$	98.2249

On the final test, the first person raised one leg and both arms and a second person lifted the robot in order to perform an intervened unstable posture Figure 13. The robot final posture and the 3-D reconstruction are shown in Figure 15 and Figure 16, respectively. The Table 6 contains the errors from each limb's angle.



**Figure 14.** Intervened unstable posture-Human pose



**Figure 15.** Intervened unstable posture-NAO pose

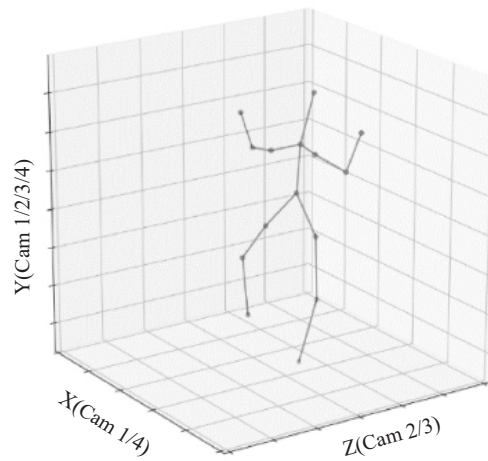


**Figure 16.** Intervened unstable posture-3-D skeleton

**Table 6.** Errors in Intervened unstable posture

Part	Axis/ID right part	Error Person-NAO (%)	Axis/ID left part	Error Person-NAO (%)
Shoulder	$Xq_1-k_1$	13.1688	$Xq_9-k_9$	12.4269
	$Yq_2-k_2$	26.2602	$Yq_{10}-k_{10}$	22.1812
	$Zq_3-k_3$	16.9042	$Zq_{11}-k_{11}$	2.5673
Elbow	$Xq_4-k_4$	12.7722	$Xq_{12}-k_{12}$	10.7212
Hip	$Yq_5-k_5$	11.5340	$Xq_{13}-k_{13}$	1.6981
	$Xq_6-k_6$	6.2620	$Xq_{14}-k_{14}$	9.1534
Knee	$Yq_8-k_8$	68.4082	$Xq_{16}-k_{16}$	28.0653

Finally, the Average Relative Errors for each test was calculated and shown in the Table 7.

**Table 7.** Relative Errors for Real Posture-NAO Robot

Test	Average Relative Errors Person-NAO (%)
Test 1	15.08
Test 2	43.20
Test 3	17.43

Only the Average Relative Errors of the arms was used to compared with the results of the state of the art, due the total error of the posture was not included as a result on the referenced paper. Both results are shown on the Table 8.

**Table 8.** Results of the state of the art

Method	Minimum reported error (%)
Method [18]	18
Proposed method	19

## 4. Conclusions

With the detailed information of limbs motions provided by the kinematic model was possible to estimate the joint angles without complex equations. These angles were used as control system's set points that controls the joint's motion speed. The maximum and minimum joint's angles from human and robots are slightly different, due the maximum angles that the robot can perform were lower than the angles that a human can perform. Even with this difference, the final posture errors resulted only 1% different than the result obtained in a similar work of the state of the art.

The robot's final posture from Test 3 was affected by the anti-fall safety system programmed by the manufacturer. This can be seen in the error values from the hip and knee. Due the human intervention, the robot could perform a complex posture avoiding the anti-fall safety system activation getting better errors values of the hip and knee.

The fuzzy control algorithm had a favorable performance moving smoothly the robot's limbs to the set-points. The joints speed was decreased when the angle measured by the joint sensor got close to the set-point. The fuzzy membership functions were correctly set due the maximum operation range and the speed configuration of the NAO limbs were knew that are included in the technical documentation of the manufacturer.

The proposed method in this paper, the 3-D analysis of the person posture was made with the information of 4 plain images from different points of view. Hence, the 3-D location of the joints are more reliable than the method where the 3-D location is estimates using only one image. Furthermore, the limitation which the person's joints must be located in front of 2 sensor was eliminated.

The artificial intelligence algorithm [16] provided the joints location no matter where the person was located on the range of the 4 cameras. The measurements were not affected by the lighting changes due the artificial intelligence algorithm was trained with different kind of images, those images included bright and dark images.

The future research will be focused on test and develop new deep learning models and fuzzy control algorithms to improve the measurement of human limbs and motion control, also the hands and finger motion will be included on the future 3-D models. The main application to focus will be the medicine and mining.

For medicine, the application to focus will be the surgeon robotics. Nowadays, the surgeon robots are teleoperated through haptic devices and specialist surgeons require many training hours to properly operate it. The motion capture through computer vision to teleoperate a robot will reduce the training time, due the surgeons will need only move their hands as they normally do at surgeon procedure, the haptic devices are not going to be required anymore.

## Conflict of interest

The authors declare no competing financial interest.

## References

- [1] Stoddard B, Cravetz M, Player T, Knight H. A haptic multimodal interface with abstract controls for semi-autonomous manipulation. In: *Proceedings of the 2022 ACM/IEEE International Conference on Human-Robot Interaction*. IEEE Press; 2022. p.1206-1207.
- [2] Puruhita ST, Satria NF, Hanafi N, Kusumawati E. Development of teleoperation humanoid robot hand mimicking through human hand Movement. In: *2020 International Electronics Symposium (IES)*. IEEE; 2020. p.277-283.
- [3] Milstein A, Alyagon L, Nisky I. Grip force control during virtual interaction with deformable and rigid objects via a haptic gripper. *IEEE Transactions on Haptics*. 2021; 14(3): 564-576.
- [4] Kaushik R, Simmons R. Perception of emotion in torso and arm movements on humanoid robot quori. In: *Companion of the 2021 ACM/IEEE International Conference on Human-Robot Interaction*. Association for Computing Machinery; 2021. p.62-66.
- [5] Yazdani A, Novin RS. Posture estimation and optimization in ergonomically intelligent teleoperation systems. In: *Companion of the 2021 ACM/IEEE International Conference on Human-Robot Interaction*. Association for Computing Machinery; 2021. p.604-606.
- [6] Lin TC, Krishnan AU, Li Z. Shared autonomous interface for reducing physical effort in robot teleoperation via

- human motion mapping. In: *2020 IEEE International Conference on Robotics and Automation (ICRA)*. IEEE; 2020. p.9157-9163.
- [7] Alquisiris-Quecha O, Maldonado-Reyes AE, Morales EF, Sucar LE. Teleoperation and control of a humanoid robot nao through body gestures. In: *2018 Seventeenth Mexican International Conference on Artificial Intelligence (MICAI)*. IEEE; 2018. p.88-94.
- [8] Torielli D, Muratore L, Laurenzi A, Tsagarakis N. TelePhysical operation: Remote robot control based on a virtual “Marionette” type interaction interface. *IEEE Robotics and Automation Letters*. 2022; 7(2): 2479-2486.
- [9] Wang Y, Zhang X, Li K, Wang J, Chen X. Humanoid robot control system Based on AR-SSVEP. In: *Proceedings of the 2020 6th International Conference on Computing and Artificial Intelligence*. Association for Computing Machinery; 2020. p.529-533.
- [10] Huang B, Timmons NG, Li Q. Augmented reality with multi-view merging for robot teleoperation. In: *Companion of the 2020 ACM/IEEE International Conference on Human-Robot Interaction*. Association for Computing Machinery; 2020. p.260-262.
- [11] Wallace D, He YH, Vaz JC, Georgescu L, Oh PY. Multimodal teleoperation of heterogeneous robots within a construction environment. In: *2020 IEEE/RSJ International Conference on Intelligent Robots and Systems (IROS)*. IEEE; 2020. p.2698-2705.
- [12] M LN, Dajles D, Siles F. Teleoperation of a humanoid robot using an optical motion capture system. In: *2018 IEEE International Work Conference on Bioinspired Intelligence (IWOBI)*. IEEE; 2018. p.1-8.
- [13] Elbeidey S, Jadhav A, Liu D, Williams T. Robot Teleoperation interfaces for customized therapy for autistic children. In: *Proceedings of the 2022 ACM/IEEE International Conference on Human-Robot Interaction*. IEEE Press; 2022. p.750-753.
- [14] Elbeidey S, Rosen D, Liu D, Shick A, Williams T. Analyzing teleoperation interface usage of robots in therapy for children with autism. In: *Proceedings of the 20th Annual ACM Interaction Design and Children Conference*. Association for Computing Machinery; 2021. p.112-118.
- [15] Elbeidey S, Shick A, Williams T. Teleoperation interface usage in robot-assisted childhood asd therapy. In: *Companion of the 2021 ACM/IEEE International Conference on Human-Robot Interaction*. Association for Computing Machinery; 2021. p.162-166.
- [16] Cruz-Silva JE, Montiel-Pérez JY, Sossa-Azuela H. 3-D human body posture reconstruction by computer vision. In: Martínez-Villaseñor L, Batyrshin I, Marín-Hernández A. (eds.) *Advances in Soft Computing*. Springer International Publishing; 2019. p.579-588.
- [17] Faller A, Schuenke M. *The Human Body: An Introduction to Structure and Function*. Thieme; 2011.
- [18] Zuher F, Romero R. Recognition of human motions for imitation and control of a humanoid robot. In: *2012 Brazilian Robotics Symposium and Latin American Robotics Symposium*. IEEE; 2012. p.190-195.